Supporting Information for:

Adsorption-Induced Conformational Isomerization of Alkyl-Substituted Thiophene Oligomers on Au(111): Impact on the Interfacial Electronic Structure

Benjamen N. Taber[†], Dmitry A. Kislitsyn[†], Christian F. Gervasi[†], Stefan C. B. Mannsfeld[‡], Lei Zhang[§], Alejandro L. Briseno[§], and George V. Nazin[†,*]

†Department of Chemistry and Biochemistry, University of Oregon, 1253 University of Oregon Eugene, OR 97403, United States

‡Center for Advancing Electronics Dresden, Dresden University of Technology, 01062 Dresden, Germany

§Department of Polymer Science and Engineering, University of Massachusetts-Amherst, Silvio O. Conte National Center for Polymer Research, 120 Governors Drive Amherst, MA 01003, United States

Corresponding Author

*E-mail: gnazin@uoregon.edu

EXPERIMENTAL METHODS

Experiments were carried out in a home-built ultra-high vacuum (UHV) cryogenic (closed-cycle cryostat-based) STM system incorporating a STM scanner from RHK Technology.[1] A Au(111)/mica substrate was prepared in situ by using multiple sputter/anneal cycles. 3,3‴-Didodecyl 2,2′:5′,2″:5″,2‴ −quaterthiophene (DDQT) molecules were prepared by Briseno et al.[2] DDQT molecules were deposited at ultra-high vacuum via in situ sublimation on to a clean Au surface. Scale was determined by atomic resolution of Au(111) lattice.

SCANNING TUNNELING SPECTROSCOPY

In constant-current mode, a scanning tunneling microscope (STM) can image the topography of a sample by recording the changes in z-height necessary for maintaining a constant tunneling current as the tip rasters across the surface of the sample. For scanning tunneling spectroscopy (STS), the STM is used in constant-height mode, with the STM tip held in a constant position (x, y, and z) while the applied bias is varied. In this work, STS measurements were carried out using the lock-in technique, with a modulation frequency of 570 Hz. This allows for the direct measurement of the differential conductance (dI/dV) of the sample at that spatial location, giving a measurement of the local density of states.[3]

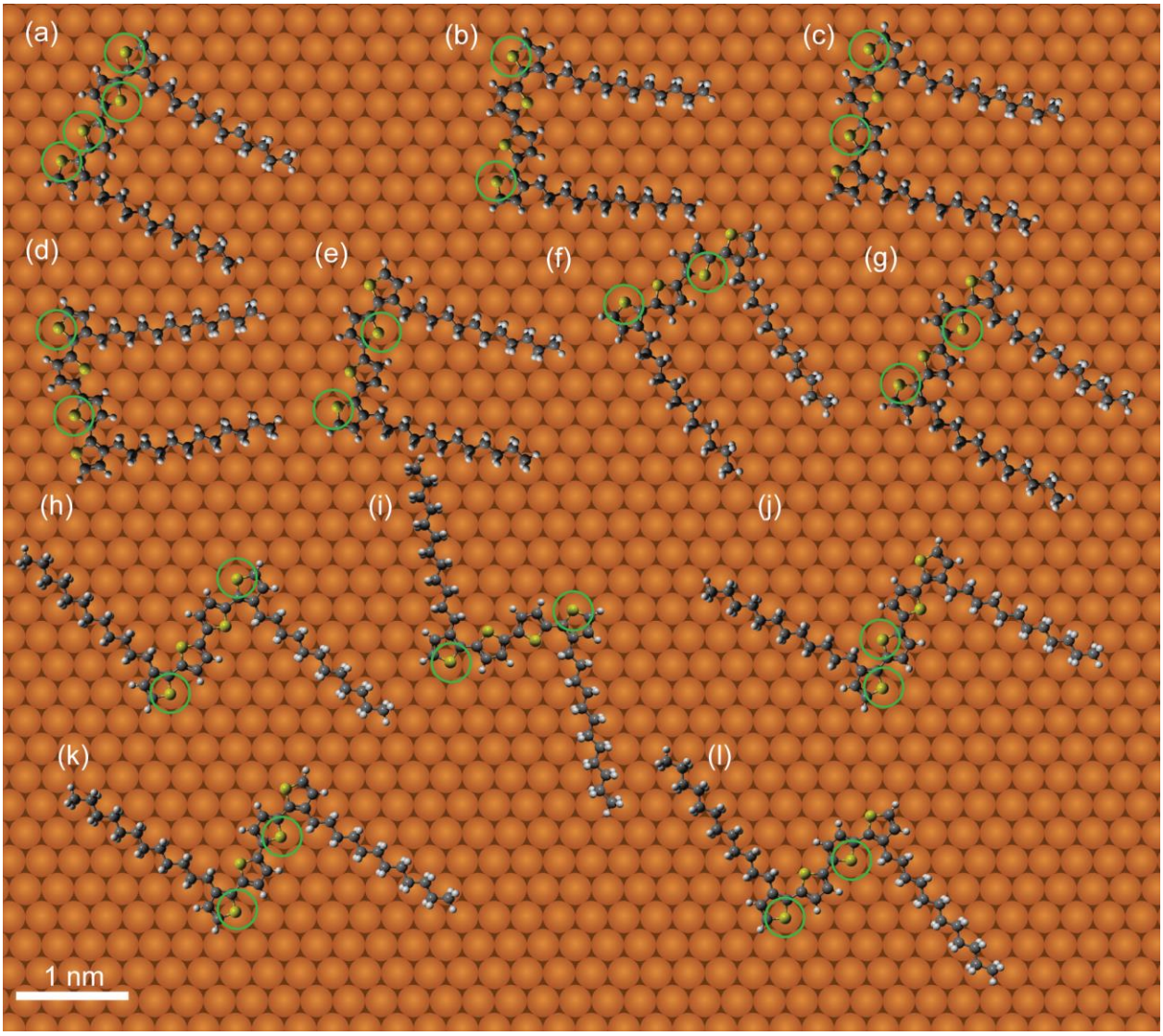

Figure S1

Possible adsorption configurations for DDQT conformers in the main text. S atoms at Au top-sites are highlighted by green circles. (a) *cis*-DDQT conformer with S atoms at Au top-sites as observed in this letter along with other possible orientations with (b) both exterior S atoms at Au top-sites and (c)-(g) one exterior and one interior S atom at Au top-sites. (h) *trans*-DDQT conformer with exterior S atoms at Au top-sites as observed in this letter along with other possible orientations with (i) both exterior S atoms at Au top-sites, (j) adjacent interior and exterior S atom in Au top-sites (this is the only possibility for *trans*-DDQT having neighboring S atoms located at Au top-sites), and (k) and (l) non-adjacent interior and exterior S atoms at Au top-sites.

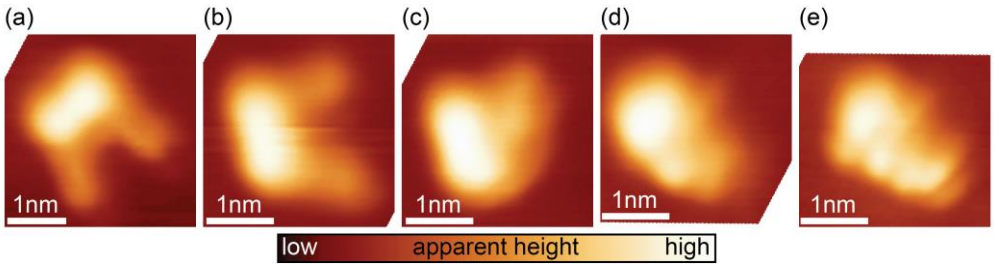

Figure S2

Manipulation of *cis*-DDQT monomer and alkyl side chains with STM tip. After the initial topography (a), the DDQT monomer rotated by 60° on the substrate (b). Subsequent STS measurements of this *cis*-conformer resulted in the alkyl chains folding over themselves (c) and the DDQT backbone (d)-(e). Topographies acquired at 1.0 V bias, 5.0 pA set point.

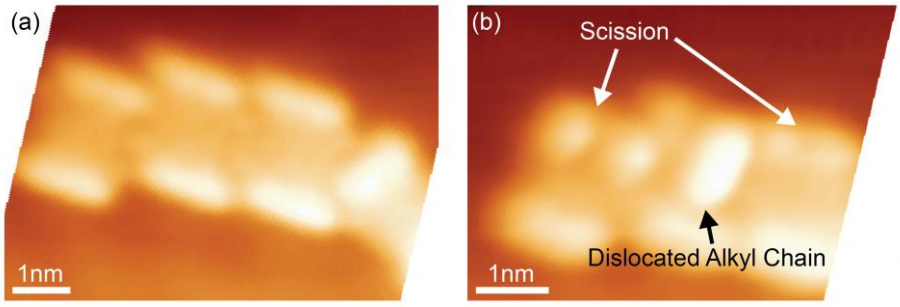

Figure S3

Examples of scission observed during STS at higher (~2.5-3.0 V) bias. Topographies (a) before STS, and (b) after. This susceptibility of DDQTs to scission limited the lifetime of individual DDQT *cis*-conformers and inhibited detailed study of unoccupied states beyond the LUMO. In addition to the scission of DDQT backbones, alkyl side chains could also dislocate from the stable dimer position (b). STM topographies were acquired at 100 mV bias, 5.0 pA set point.

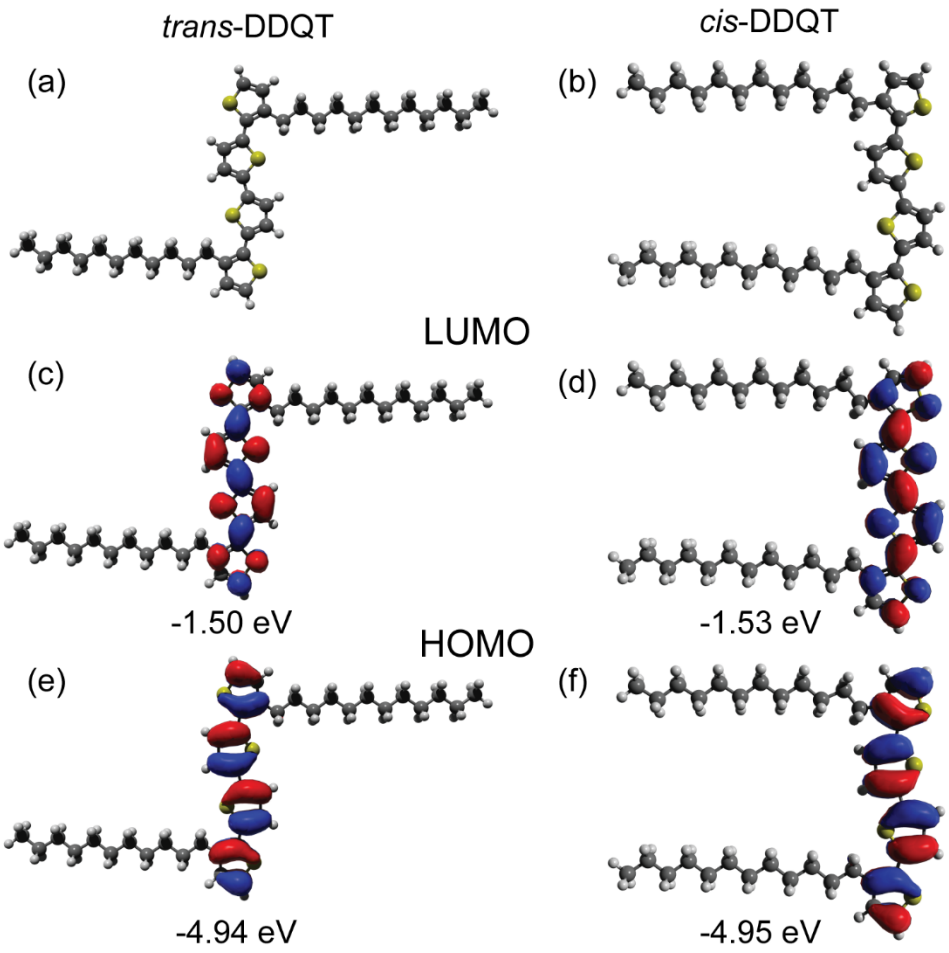

Figure S4

Density Functional Theory gas-phase electronic structure calculations of (a) *trans* DDQT and (b) *cis* DDQT. (c) and (d) LUMOs and their energies for *trans* and *cis* conformers, correspondingly. (e) and (f) HOMOs and their energies for *trans* and *cis* conformers, correspondingly. The dipole moment of the *trans* (*cis*) conformation is 0.06 Debye (2.32 Debye). Computations were performed with Gaussian09[4] using B3LYP/6-31G* and visualized with Avogadro[5].

Functional	DDQT Conform-ation	HOMO (eV)	LUMO (eV)	HOMO-LUMO Gap (eV)	Dipole Moment (Debye)
B3LYP	*cis*	-4.95	-1.53	3.41	2.32
	trans	-4.94	-1.50	3.45	0.06
PBE	*cis*	-4.37	-2.06	2.31	2.46
	trans	-4.36	-2.03	2.34	0.06
PW91	*cis*	-4.40	-2.10	2.30	2.45
	trans	-4.39	-2.07	2.33	0.06

Table S1

Frontier orbital energies and dipole moments from DFT calculations using the B3YLP[6,7]—a non-local (hybrid) functional—and PBE[8] and PW91[9]—semi-local exchange-correlation functionals. The calculated dipole moments of *cis*-DDQT (2.3-2.5 Debye) were significantly greater than that of *trans*-DDQT (0.06 Debye), leading to the enhanced interaction of the *cis*-conformer with image charges at the metal surface. In all three calculations, the *cis*-LUMO was found to be higher (by ~30 meV) than the *trans*-LUMO. All DFT computations used the 6-31G* basis set.

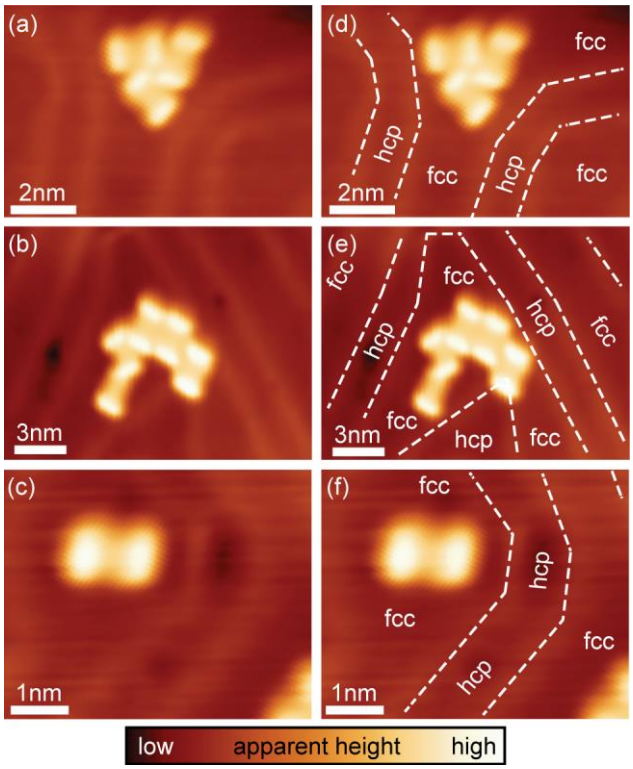

Figure S5

Registry of DDQT molecules with the underlying Au(111) surface as in Figure 2 of the main text, with surface reconstruction ridges highlighted by white dashed lines delineating face-centered-cubic (fcc) and hexagonal-close-packed (hcp) regions of the Au(111) surface (d)-(f). (a)-(c) STM images of DDQT molecules on Au(111) substrate. DDQT molecules primarily adsorbed in the fcc regions, with the quaterthiophene backbones aligned along one of three ⟨110⟩ directions of the Au(111) surface, perpendicular to Au(111) surface reconstruction ridges aligned primarily along the ⟨112⟩ directions, as shown in Figure 2 (main text). STM imaging was carried out at bias voltages 0.1-1.0 V and tunneling currents 1-5 pA.

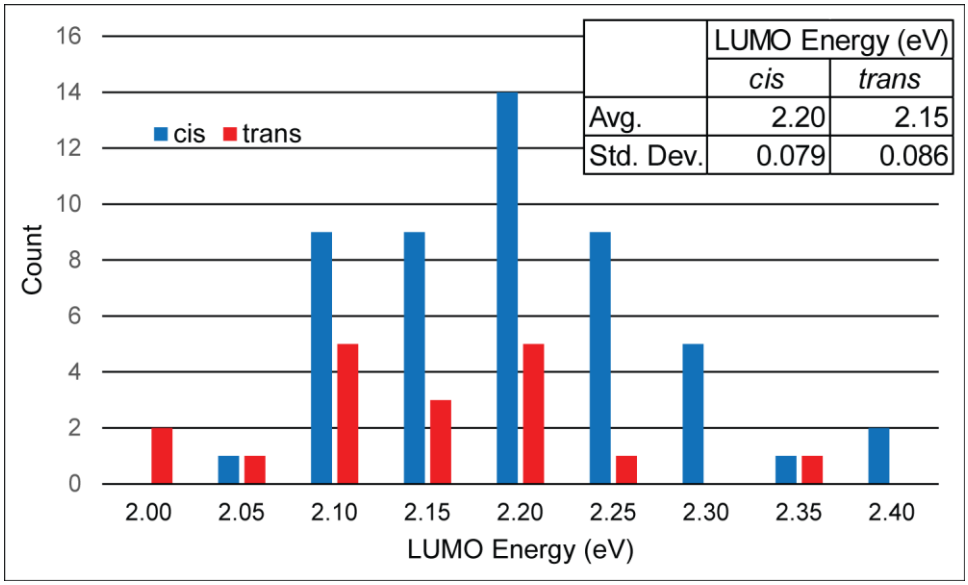

Figure S6
Distributions of LUMO energies for 50 *cis* and 18 *trans*-conformers, as measured by STS.

References

(1) Hackley, J. D.; Kislitsyn, D. A.; Beaman, D. K.; Ulrich, S.; Nazin, G. V. High-Stability Cryogenic Scanning Tunneling Microscope Based on a Closed-Cycle Cryostat. *Rev. Sci. Instrum.* **2014**, *85*, 103704.

(2) Zhang, L.; Colella, N. S.; Liu, F.; Trahan, S.; Baral, J. K.; Winter, H. H.; Mannsfeld, S. C. B.; Briseno, A. L. Synthesis, Electronic Structure, Molecular Packing/Morphology Evolution, and Carrier Mobilities of Pure Oligo-/Poly(alkylthiophenes). *J. Am. Chem. Soc.* **2012**, *135*, 844-854.

(3) Chen, C. J. *Introduction to Scanning Tunneling Microscopy*; Second Edition ed.; Oxford University Press: New York, 2008.

(4) Gaussian 09, Revision C.01, Frisch, M. J.; Trucks, G. W.; Schlegel, H. B.; Scuseria, G. E.; Robb, M. A.; Cheeseman, J. R.; Scalmani, G.; Barone, V.; Mennucci, B.; Petersson, G. A. et al. Gaussian, Inc., Wallingford CT, **2009**.

(5) Hanwell, M. D.; Curtis, D.; Lonie, D.; Vandermeerschd, T.; Zurek, E.; Hutchison, G. Avogadro: an Advanced Semantic Chemical Editor, Visualization, and Analysis Platform. *J. Cheminform.* **2012,** *4***,** 1–17.

(6) Becke, A.D. Density-Functional Thermochemistry. III. The Role of Exact Exchange. *J. Chem. Phys.* **1993**, *98*, 5648-5652.

(7) Stephens, P.J.; Devlin, F.J.; Chabalowski, C.F.; Frisch, M.J.; Ab Initio Calculation of Vibrational Absorption and Circular Dichroism Spectra Using Density Functional Force Fields. *J. Phys. Chem*. **1994**, *98*, 11623-11627.

(8) Perdew, J. P.; Burke, K.; Ernzerhof, M.; Generalised Gradient Approximation Made Simple. *Phys. Rev. Lett.* **1996**, *77*, 3865-3868.

(9) Perdew, J. P.; Wang, Y.; Accurate and Simple Analytic Representation of the Electron-Gas Correlation Energy. *Phys. Rev. B* **1992**, *45*, 13244-13249.